Short communication

Microstructural characterization of *Zr1Nb* alloy after hot rolling

Armando C. Souza[a,b], Flavio Aristone[c,*], Jesualdo L. Rossi[b], Luis G. Martinez[b], Franciso C. Cione[b], Panos Tsakiropoulos[d], Carlos R. Grandini[e], Wallace F. da Silva[c]

[a] *UEMS, Department of Physics, CP 351, 79804-970 Dourados, MS, Brazil*
[b] *IPEN, Center of Technology, Science and Materials, 05508-000 Sao Paulo, SP, Brazil*
[c] *UFMS, Institute of Physics, 79070-900 Campo Grande, MS, Brazil*
[d] *University of Sheffield, Department of Materials Science and Engineering, Sheffield S1 3JD, UK*
[e] *UNESP, Department of Physics, UNESP, 17.033-360, Bauru, SP, Brazil*

ABSTRACT

The nuclear industries have large interest on the development of new alloys involving zirconium (*Zr*) because this material presents extraordinary mechanical properties, outstanding resistance to corrosion and high permeability to thermal neutrons, being suitable for applications in areas such as energy and human health. The alloy studied in this paper is formed by *Zr* and niobium (*Nb*), normally expressed as *Zr1Nb*. These two elements have large chemical affinities with oxygen, carbon, and nitrogen, elements that normally are responsible for a series of damages in the alloy. The principal goal of this work is to obtain *Zr1Nb* alloys and to perform microstructural characterizations before and after the hot rolling process. The resulting alloys were subjected to a process of heat treatment, the temperature was increased at a rate of 10 K/min up to 1273 K and maintained for 2 h, after which it was cooled down at −10 K/min until room temperature, with the only purpose of relieving residual stresses. The next step was to apply the hot rolling process to the alloy. The sample initially measured, approximately, 1.5 cm of thickness when it was inserted into the furnace at 1203 K to start the hot rolling. Every pass on the hot rolling reduced the thickness by 0.5 mm, originating uniform and homogeneous samples of 2.5 mm thickness. Auxiliary technical tools, such as XRD (X-Ray Diffraction), SEM (Scanning Electron Microscopy), and EDS (Energy Dispersive X-Ray Spectroscopy), were used to analyze the microstructure of the samples before and after the hot rolling process. The XRD results show the formation of only a single α-HCP (Hexagonal Close Packed) phase for our samples, indicating that they are free of other phases that can damage the material. This result is consistent and coherent with both SEM and EDS analysis. The observed homogeneity of our samples is very good; proving that both techniques employed to obtain *Zr1Nb* as well as the hot rolling process was well succeeded. Therefore, the obtained alloy can be directly used in the pipes of nuclear combustible industries.

1. Introduction

Metal rolling is one of the most important steps among the processes of manufacturing materials for general applications. The large majority of currently metallic products are subject to the process of metal rolling at a determined point during their manufacturing. Generally, metal rolling is the first step in creating raw metal forms. The basic structures for creation of a wide range of manufactured forms are the ingot or hot rolled continuous casting in the form of bloom or slab.

Blooms have a square cross section typically larger than 6 × 6 in. (150 × 150 mm). Slabs are rectangular and are usually thicker than 1.5 in. (38 mm) and longer and wider than 10 in. (250 mm). The process

of rolling is most often performed hot, particularly in the case of ingot conversion on continuous casting.

At a rolling mill, blooms and slabs are further rolled down to intermediate parts such as plate, sheet, strip, coil, billets, bars and rods. Many of these products will originate materials for subsequent manufacturing operations such as forging, sheet metal working, wire drawing, extrusion, and machining. Blooms are often rolled directly into I or H beam shapes, channel beams, or T section shapes for structural applications. Rolled bars of various shapes and specific cross sections are used in the machine building industry, as well as at the construction sector. Rails to be used as railroad tracks are also rolled directly from blooms. Plates and sheets rolled from slabs are extremely

---

important in the production of a wide range of manufactured items. Plates are generally over 1/4″ or 6 mm in thickness and used in heavy applications such as boilers, bridges, nuclear vessels, large machines, tanks and ships. Sheets are used for the production of car bodies, buses, train cars, airplane fuselages, refrigerators, washers, dryers, other household appliances, office equipment, containers, and beverage cans, to name a few examples. It is remarkable the significance of metal rolling in industry nowadays, as well as its integration with other manufacturing processes.

The need and interest to fully understand the behavior and performance of Zr alloys for nuclear applications has been growing in recent years due to several factors. The development of new reactors for different operating conditions aims to minimize the cyclic costs of continuous fuel thru the demand for structural materials. Therefore, phenomena of corrosion and deformation of materials are frequently studied, principally in the sector of processed Zr alloys to be used in nuclear applications [1,2].

In the metallurgical sector, several researches follow the direction of quantifying the precipitation of second phase β Nb particles: the sample texture changes; the transformations of α-β-α phases; the displacement and concentration of defects; etc. All dynamic recrystallizations occur very rapidly during the processes involved in the production of alloys. The importance of knowing and establishing parameters to process Zr alloys is therefore evidenced [3,4]. According to the literature, Zr alloys exhibit significant amounts of second phase precipitates, such as formation of oxides, carbides and nitrides. Oxides occur when the amount of oxygen in mass is between 6.6% and 26%, for temperatures above 200 °C; carbides occur when the amount of carbon is 7.5% for temperatures above 500 °C; nitrides occur when nitrogen is between 0.8% and 3.0% for temperatures above 700 °C.

Currently, zirconium ranks eighteenth in abundance on Earth's crust, being found in larger quantity than copper, lead and zinc, among others. The main application of Zr alloys is as elements of fuel cells for nuclear reactors [5], representing about 90% of all of it. These applications are due to its small cross-section when capturing thermal neutrons and to its excellent resistance to corrosion [6]. In industry, Zr is used as an additive for production of steel in order to obtain materials with high mechanical resistance. Nickel alloys are similar and/or equivalent materials to Zr alloys. They are frequently employed in the chemical industry due to their high resistance to corrosion in acid medium [7].

Niobium is a refractory metal for which the melting point is 2750 K. It has excellent mechanical properties, such as stiffness, hardness, thermal and chemical stability, it is resistant to corrosion and to fatigue, and it is biocompatible. Its density is $8.75 \, g/cm3$ and it has a high ductility compared to most metals. Inside an alloy, the niobium enters as a substitutional element in an array forming the crystal structure of zirconium, originating the Zr1Nb alloy [8,9].

The principal goal of this work is to obtain Zr1Nb alloys through high-temperature fusion, making use of a non-consumable electrode furnace, and to perform a series of microstructural characterizations in these alloys before and after they are submitted to the hot rolling process. Commercial Zr and Nb materials were weighted and melted. In order to realize the zirconium and niobium fusion it is necessary to determine the working conditions of the melting furnace as a function of a series of parameters. The most important parameters to be considered are: the melting flow and the pressure of the inert gas atmosphere that is required for the fusion process [10,11].

The resulting alloys were then subjected to a heat treatment process with the only purpose of relieving residual stresses. This choice of temperature limit is enough to avoid oxidation and consequently absorption of hydrogen by the alloys. The next step was the application of the hot rolling process on the resulting alloy, in order to obtain uniform and homogeneous samples having 2.5 mm thickness.

Microstructural characterizations of these Zr1Nb alloys have been done through conventional X-ray diffractions, optical microscopy, and scanning electron microscopy [12]. The samples were investigated before and after the hot rolling to analyze the microstructure of the resulting surface in terms of texture, plastic deformations, and precipitates. The precipitation phase as well as defects of dislocation attributed to the process of hot rolling contribute directly to the deterioration of mechanical properties and performance against corrosion of the Zr1Nb alloys. The interest of this work on the analysis and comprehension of the microstructural evolution for such high performance alloys used for application in nuclear reactors is therefore vastly justified [13].

2. Material and methods

The samples of polycrystalline Zr used to obtain the results hereby described have been commercially acquired in cylindrical form. Polycrystalline samples of Nb were obtained thru electron beam melting and supplied to study as triangular bars of 15 cm long, provided by the Lorena School of Engineering, University of Sao Paulo, Brazil.

The furnace used to process the alloys of Zr1Nb melts non-consumable electrode arcs under inert gas atmosphere. It is a V-series II manufactured by Materials Research Corporation. The vacuum system consists of a mechanical pump by Edwards, model A65201903, with a pumping capacity of $4.5 \, m^3/h$ and pressure limit on the order of 10^{-3} Torr. The rectifier model R-400 by Hobart Brothers Welding Co. shown in Fig. 1 provides the necessary energy for melting.

A heat treatment of the samples was applied after the alloy was melted. An ultra-high-vacuum system of the Inelastic Relaxations Laboratory of the Department of Physics, State University of Sao Paulo (UNESP), at the city of Bauru, State of Sao Paulo, Brazil was used. A schematic drawing is represented in Fig. 2, see also reference [14]. Our heat treatment process consists on placing the sample in a vacuum system at 10^{-4} Torr, with an applied heating temperature ramp of 10 K/min until it reaches 1273 K, where it was kept for 2 h. Such a temperature is clearly smaller than the temperature necessary for melting. After this plateau, the sample is cooled down to room temperature again, at a maximum rate of -10 K/min. Such a heat treatment has the only purpose of minimizing residual tensions and to allow a better distribution of grains.

The hot rolling process used a FENN brand two cylinders laminator that belongs to the Center of Materials and Technology of the Brazilian Institute for Energy and Nuclear Research – IPEN. The system is schematically represented in Fig. 3. Before starting the rolling process, the sample was inserted in a copper pipe lately melted on its extremities to minimize oxidation and kept inside a furnace at 1203 K. The sample thickness was reduced 0,5 mm on every passage of the sample in the laminator. Each sample had initially 1.5 cm thickness approximately, and then it was rolled down to 2.5 mm. After each rolling step, the sample was reinserted into the furnace for 1 min, in order to stabilize the temperature.

All samples have been prepared at the facilities of the "Center of Characterization and Materials Technology" of IPEN. After being embedded, these alloys were initially polished and then analyzed using a Scanning Electron Microscopy (SEM) with an Energy Dispersive Spectroscopy (EDS) system attached. This system is a JEOL 5800 LV equipment located at the Institute of Physics (INFI) of the South Mato Grosso Federal University (UFMS), Brazil. Measurements of X-ray diffraction have been realized at the Powder X-ray Diffraction (XPD) light station of the Brazilian National Synchrotron Light Laboratory (LNLS). A monochromatic detector Mythen at 1550.3939 Å wavelength, sensitive to the linear position, was used.

3. Results and discussions

3.1. Determination of the parameters of fusion

The Zr1Nb samples used here in this paper to study the

Fig. 1. Pictures of the furnace-gas-rectifier ensemble used to produce *Zr1Nb alloys*.

microstructural evolution after the procedure of hot rolling were all submitted to the same treatment described by Souza et al [12]. The experimental parameters were determined individually for each type of furnace. Several individual tests were performed using an Argon S type cylinder and various samples have been measured, weighting approximately 50 g each.

During the development of tests to determine the optimal current range for the fusion process, a few samples released vapors that interfered with the performance of the arc furnace, blurring the observation window, thereby hindering the absolute control of the melting process. After all initial tests, the ideal interval of current range was observed to vary from 100 to 300 A. The value of $I = 275$ A generated the best results to melt the alloys.

After initial tests were ran, both the optimized pressure of the inert gas that is required during the melting process inside the furnace chamber as well as the best vacuum pressure before melting were determined. When running tests, the vacuum pressure prior to the melting process has been stablished as 6.35×10^{-2} Torr, while the pressure of the inert gas during melting was around 5.58×10^{-2} Torr. These conditions were adequate to maintain an open-loop stability with excellent efficiency for the setting of the melting process.

Before starting the process of melting, the system was purged with argon gas three times. For each purge, Argon gas was injected until the vacuum pressure was reduced to 2.54×10^{-2} Torr. Such injection is designed to prevent impurities from the external atmosphere that could contaminate the samples during the purges. After the melting is
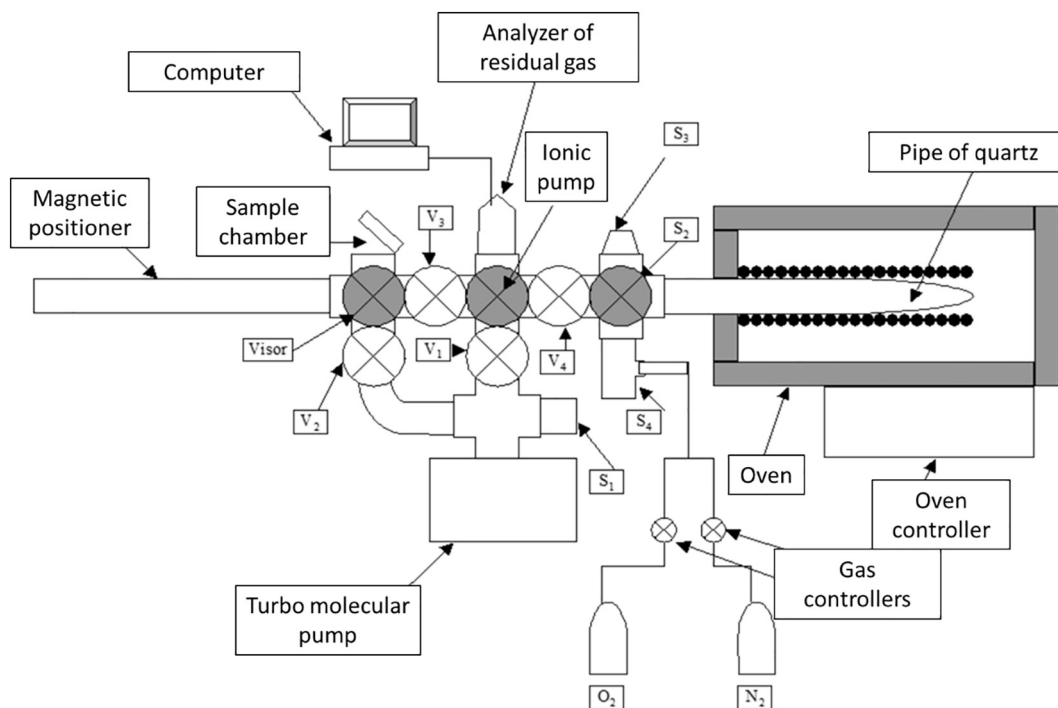

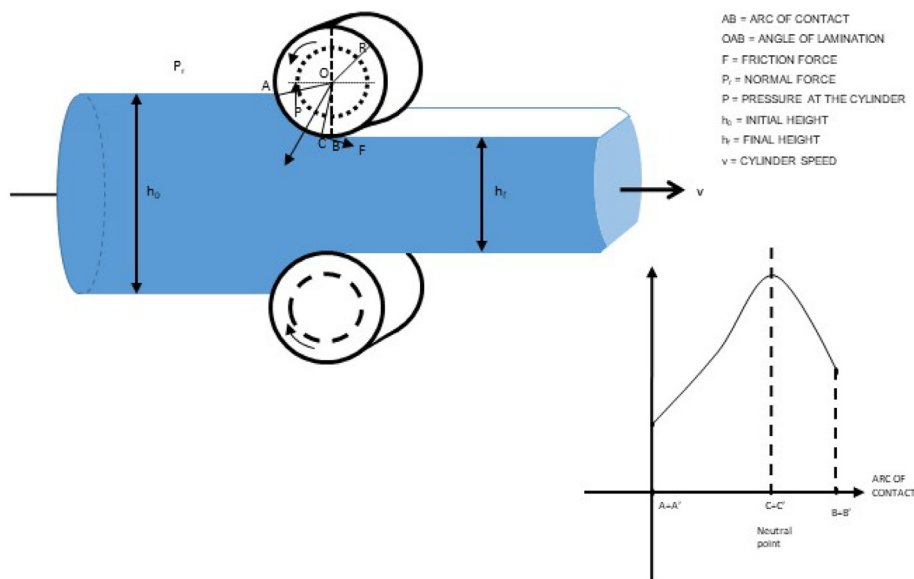**Fig. 2.** Schematic diagram of the thermal treatment system.

AB = ARC OF CONTACT
OAB = ANGLE OF LAMINATION
F = FRICTION FORCE
P_r = NORMAL FORCE
P = PRESSURE AT THE CYLINDER
h_0 = INITIAL HEIGHT
h_f = FINAL HEIGHT
v = CYLINDER SPEED

Fig. 3. Schematic representation of the strengths involved during a process of rolling and some geometric relations.
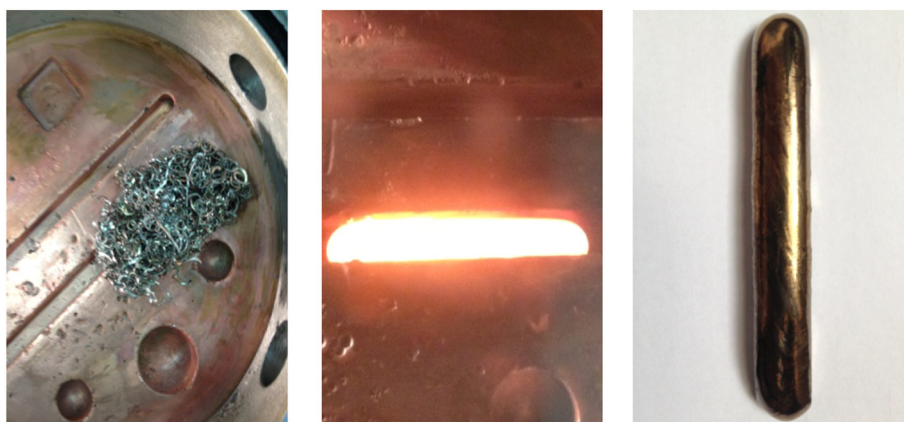

Fig. 4. Sequence of preparation and acquisition for the melting of a *Zr1Nb* alloy.

Table 1
Optimized results determined for the melting parameters of a *Zr1Nb* alloy.

Parameter	Used value
Pressure before melting	$6{,}35 \times 10^{-2}$ Torr
Pressure during melting	$5{,}58 \times 10^{-2}$ Torr
Pressure between purges	$2{,}54 \times 10^{-2}$ Torr
Optimized current	275 A
Cooling time	35 min
Number of purges	3

finished, the whole system is maintained under the same conditions for extra 5 min, i.e., the flow of the inert Argon gas is kept constant for such a while, exactly like during a purge. The vacuum pressure is held at 6.35×10^{-2} Torr for another 30 min before opening the furnace to accomplish the temperature cooling procedure. The samples are then cooled to avoid major contaminations either by internal or external gases present in the atmosphere. This procedure ensured the production of high-purity and homogeneous samples. A typical sample is represented in the pictures exhibited in Fig. 4. The parameters for each one of the melted alloys are shown in Table 1.

3.2. X-ray diffraction

In Fig. 5(a) and (b) are represented typical results of X-ray diffraction obtained for the *Zr1Nb* alloy, which was obtained as described in the previous section. The X-ray spectrum exhibited in Fig. 5(a) represents the analysis of the "raw" *Zr1Nb* sample, i.e., before hot rolling it. Fig. 5(a) ought to be compared directly to the spectrum shown in Fig. 5(b), which was obtained for the same sample but after a full cycle of hot rolling.

Variations on the intensity of peaks are observed when comparing these two spectra. This effect is mainly attributed to the orientation of grains in the sample before and after hot rolling treatment. The position of peaks is characteristic of a crystalline structure of HCP type. The analysis of such X-ray diagrams identifies the planes of wave reflection leading therefore to the Miller indexes. Applying the Miller indexes that were obtained to the Bragg's law for an HCP crystalline structure, the following lattice parameters are obtained: $a = 3.238527$ Å; $b = 3.238527$ Å and $c = 5.161452$ Å respectively.

During the hot rolling treatment, the sample is submitted to temperatures of 930 °C; consequently, the phenomenon of allotropic *Zr* induces the HCP crystalline phase to change into a BCC structure type. A detailed study of these charts of X-ray diffraction leads to some important conclusions. An alloy that has been submitted to the procedure of hot rolling generates an X-ray diffraction chart that does not show
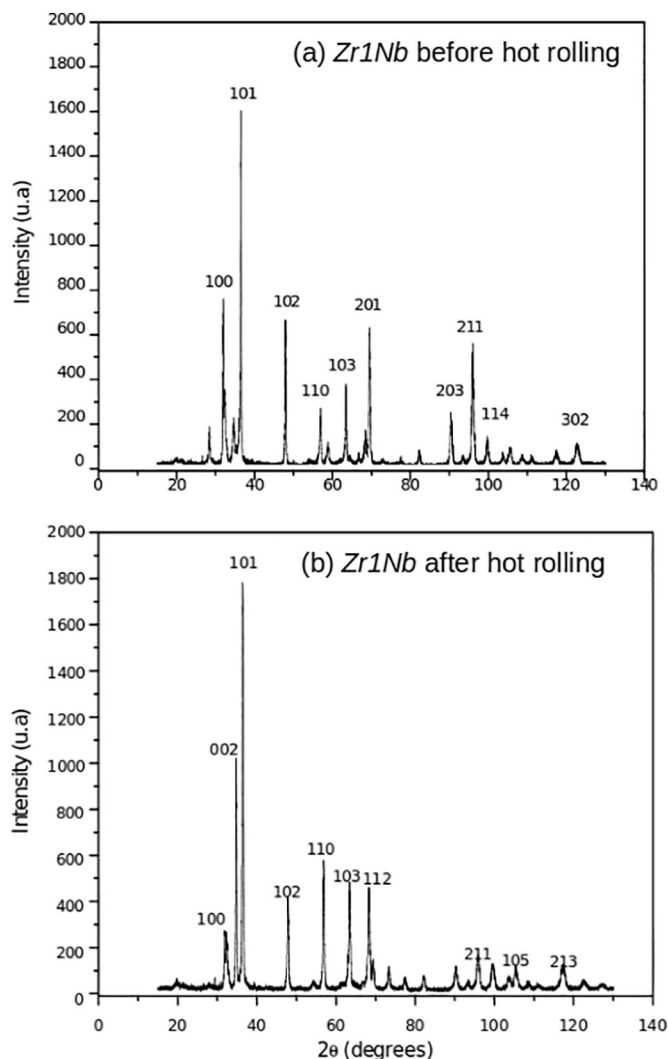
Fig. 5. a) Standard X-ray diffraction of a *Zr*1*Nb* alloy sample before it was submitted to the process of hot rolling; b) Standard X-ray diffraction of the same sample but after it was submitted to the hot rolling procedure.

precipitation of any one of the following phases: β-*Zr*, β-*Nb* and α/(α + β). Therefore, it confirms the dissolution of *Nb* occurring as a substitutional solid solution in the crystalline structure of the *Zr* matrix. The stability of the α phase is inferred from the high reproducibility of the X-ray diffraction charts. Such a reproducibility shows that the parameters previously established, which were obtained during the rolling process, contribute directly to the optimization of manufacturing Zr1Nb alloys process, with excellent stability.

3.3. Optical microscopy

Optical microscopy was performed using a Leica microscope model LAS-EZ, with coupled digital camera and software by Leica Application. This equipment belongs to the Laboratory of Corrosion of the Center of Science and Technology of Materials (CCTM), IPEN. It was used to investigate the superficial characteristics of the sample in terms of homogeneity and distribution of particles as a function of the grain contours. Measurements were performed before and after the hot rolling process.

Two micrograph pictures are exhibited in Fig. 6(a) and (b), the first one shows the surface of the commercial *Zr* raw material while the other shows the surface of the *Nb* of nuclear grade. These materials are the precursors used to obtain the intended alloys. It is noticeable that

both surfaces present a good homogeneity for these samples. However, it also clear that the porous density is larger for *Zr* than for *Nb*.

The densities of *Zr* and *Nb* remain on the order of 6.513 and 8.575 g/cm^3 respectively. These numbers are coherent and completely in agreement with the current reference values found in periodic tables. The sample porosity is evidenced when both photomicrographs are compared. Even from this qualitative analysis, it is possible to infer that the zirconium, considered as a matrix, enhances the dissolution of oxygen and consequently also enhances the absorption of hydrogen because it has strong affinities with *O, N*, and *H*. The presence of these elements is prejudicial to the material. Dissolution of oxygen provokes a loss of ductility while absorption of hydrogen causes embrittlement due to the formation of hydrides. Therefore, the relevance on performing such studies after the hot rolling process is largely justified.

Surface effects due to the thermal (heat) treatment enforced on the *Zr*1*Nb* alloy samples are discussed based on the sequence of micrographs shown in the whole Fig. 7, which is composed of four different pictures representing the different phases of sample preparation. The micrograph picture exhibited in Fig. 7(a) was taken from the alloy directly after the fusion. The micrograph picture exhibited in Fig. 7(b) was taken after the heat treatment for homogenization and it is noticeable the growth of dendrites.

The direction of dendrites is well defined after the heat treatment, being aligned in opposite direction of the heat extraction. The boundaries of grains are also evidenced and discussed for these pictures. Before the thermal treatment, the pores were more concentrated, i.e., alternating regions of high density with regions of low density. After the sample was thermally treated though the grains became distributed much more homogenously in the whole sample surface. As a consequence, this more homogeneous distribution implies the relief of the residual tension, therefore minimizing the deformations due to the conditions of grain boundaries [15].

The micrograph exhibited in Figs. 7(c) and (d) are pictures obtained for the transverse and the longitudinal sections of the previously thermally treated sample, respectively. It is important to notice the deformation and the alignment of the dendrites shown in these pictures. A small oxidized layer also appears in these pictures.

The results exhibited in both Figs. 7(c) and (d) clearly indicates that there is a substantial affinity between *Zr* and *O*. The α phase of zirconium, simply noted by α-*Zr*, dissolves oxygen interstitially until the maximum limit of oxygen solubility, which is 35% at the eutectic temperature of 2338 K [16]. Similarly, the β phase of zirconium, or β-*Zr*, also dissolves oxygen interstitially, but the maximum limit of solubility occurs when the *O* is 10.5% at 2243 K [17].

The resulting dynamics indicate that the niobium is a substitutional element in the zirconium matrix, what is coherent with the results obtained in the diffractograms, where the indexed peaks are characteristic of the HCP crystal structure of Zr. Oxygen stabilizes the α-*Zr* phase and niobium stabilizes the β-*Zr* phase. This difference in the stability of phases results in a very small limit of oxygen solubility for the *Zr*1*Nb* alloys. The limits of solubility are quite large for β-*Nb* in a BCC structure; for α-*Zr* in an HCP structure and for β-*Zr* in a BCC structure [18].

3.4. Scanning Electric Microscopy - SEM

Microstructural analyses of the samples through SEM are discussed in this section. The same process of comparison applies again. The pictures represented in Fig. 8(a) and (b) were obtained for the surface of sample after the process of fusion only, i.e. before the hot rolling.

This picture was taken using backscattering electrons, allowing to notice the deformation of grains along the contrast depth. The average size of grains is particularly extended for this cross section of the sample that was investigated. Fig. 8(b) was taken for the same section of the same sample, but using image of secondary electrons nevertheless. Morphological aspects of the α-*Zr* phase are noticeable in this picture,

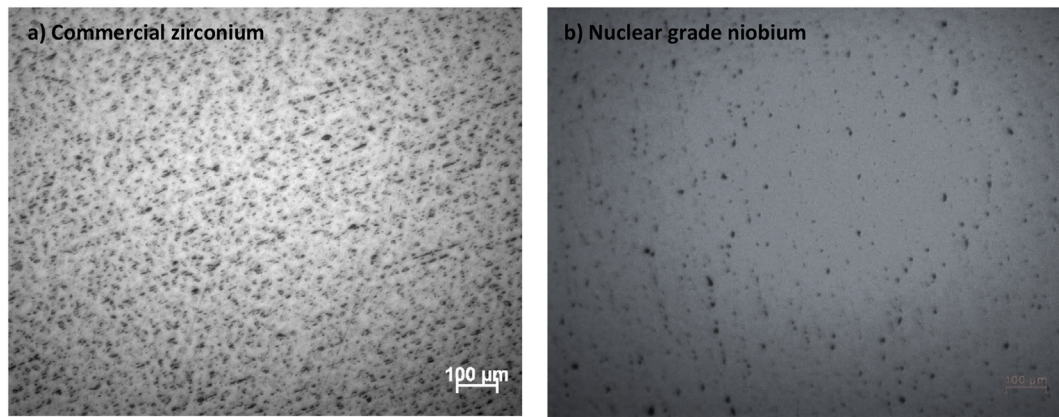**Fig. 6.** Optical photomicrograph for (a) commercial *Zr* and (b) nuclear grade *Nb*.
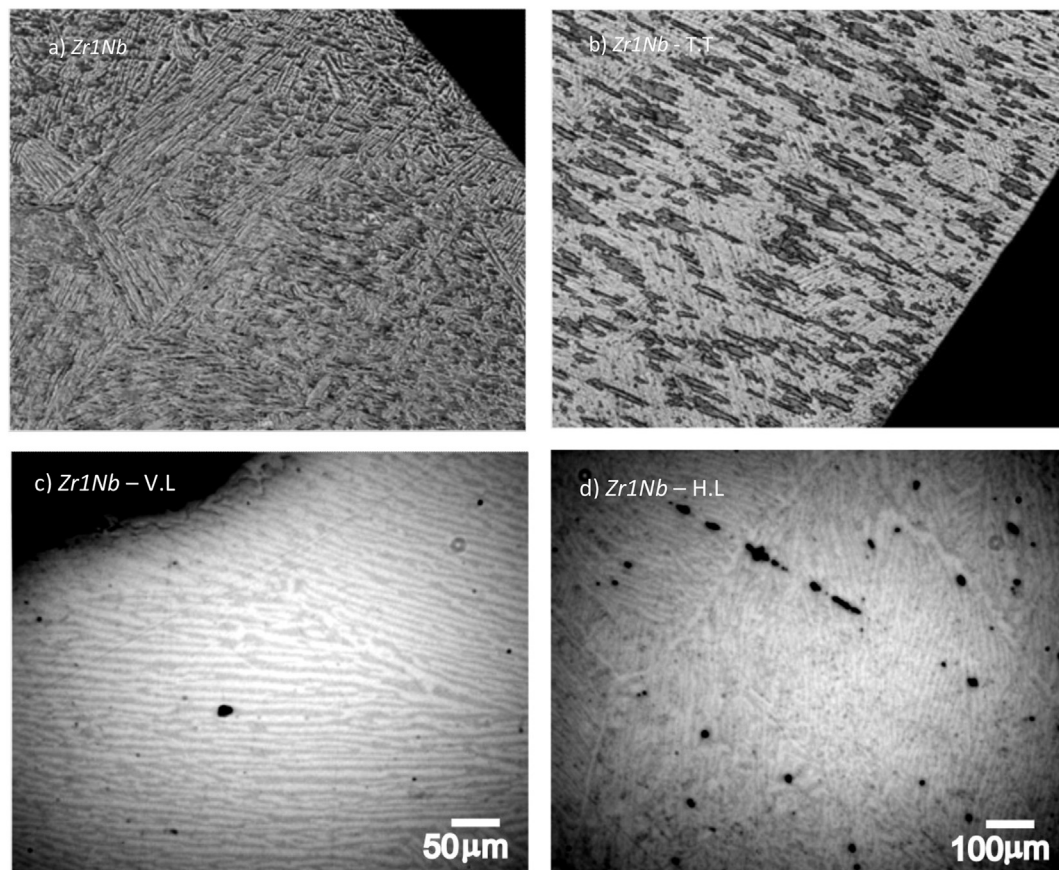

Fig. 7. A sequence of typical micrographs obtained for a sample of *Zr1Nb* alloy: (a) its surface after the fusion only; (b) the same surface but after being submitted to the heat thermal treatment; (c) the transversal section; and (d) the longitudinal section.

represented by the external appearance of the sample in terms of pore deformation and their distribution on the surface before hot rolling.

The next two pictures on Fig. 8(c) and (d) were taken for the same sample but after the sample was submitted to the hot rolling procedure. The Fig. 8(c) is to be compared to Fig. 8(a), since both were taken using backscattering electrons, as well as Fig. 8(d) is to be compared to Fig. 8(b), since both were taken using secondary electron imaging.

The pictures of the sample after thermal treatment highlight the boundaries of grains for the *Zr1Nb* alloys. The first conclusion is that the deformation of grains clearly increased on both Fig. 8(c) and (d) when compared to the previous ones, Fig. 8(a) and (b). However, it is also noticeable that the cross-section area of those grains along the rolling plan has been significantly reduced.

When looking at the ensemble of both pictures taken of the samples before and after hot rolling it becomes clear that the homogeneity for this *Zr1Nb* alloy has improved considerably. Even if the deformation of individual grains has increased after the hot rolling process, the large majority of grains have actually disappeared, leading to a much "clearer" and homogeneous sample.

A thorough analysis of the photomicrograph reveals a small region on the contour extremities of the sample with a clearer (almost white) color, which characterizes the presence of oxides. During the process of thermal treatment, oxygen spreads on the whole sample surface. According to the resulting photomicrograph, the whole sample keeps stable, as previously explained, due to the limit of solubility.

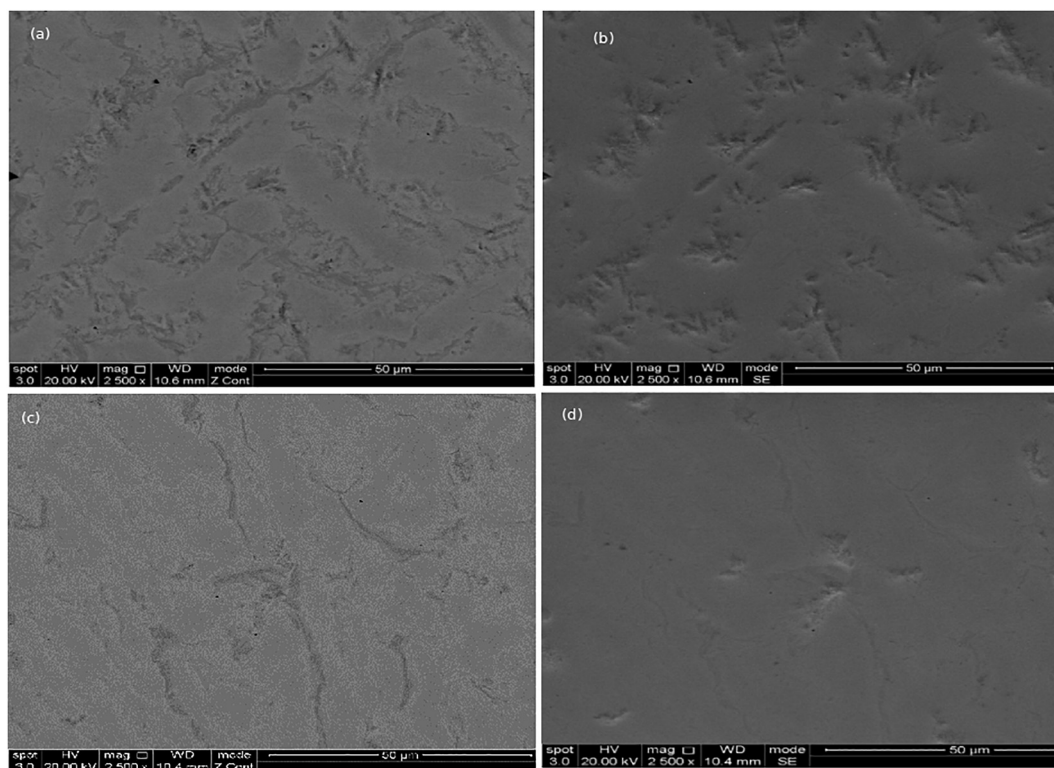The oxygen concentration measured for this sample at the boundary

Fig. 8. Results of SEM obtained for the surface of *Zr1Nb* alloy. Pictures (a) and (b) were obtained for the sample after fusion only. Pictures (c) and (d) were obtained for the sample after the thermal treatment.

of the metal-oxide phase is approximately equal to the oxygen concentration at equilibrium. The value of 6.7 in mass percentage is the upper limit of oxygen concentration for the α-*Zr* phase at the temperature interval comprised between 1223 and 2173 K [17]. Gas analysis realized at the Sheffield University-UK found the value of 0.215% in mass of Oxygen for our samples. Therefore, the working temperature of 1203 K is well established, especially after considering all images of micro-structures obtained for the studied samples. The samples that were obtained as previously described present neither α-*Zr*(O), nor β-*Zr*(O) nor hydride phase transformations. Such conclusions have been confirmed through the analyze of the pictures that were beforehand exhibited, proving that an excellent homogeneity of phases was achieved. This homogeneity is due to the presence of the niobium β-stabilizer element, which played an important role regarding the dissolution of small concentrations of oxygen and hydrogen in the solid solution of the matrix after the hot rolling process.

Results of EDS acquired for the same *Zr1Nb* sample obtained after the hot rolling processes are exhibited in Table 2. The corresponding graphics clearly show the concentrations of each element involved in the alloy. It can be noticed that the presence of the atomic *Zr* in the matrix is approximately 99.33% while the substitutional atomic *Nb* represents 0.67%. These numbers confirm a homogeneous distribution

of *Nb* as a substitutional element. The respective data were obtained for the following set of parameters: Life Time: 100.0 s.; Acc. Voltage: 30.0 kV; Take Off Angle: 37.2 deg.; Amplification: 1500×; and Detector: Pioneer.

Characterization of the sample through the measurement of the Energy Dispersive Spectroscopy (EDS) has also been done. A typical curve of EDS characterization is exhibited in Fig. 9 for the *Zr1Nb* alloy after it was submitted to the hot rolling process.

Peaks representing both *Zr* and *Nb* are present at 2.2 and 2.3 keV respectively. These peaks thus confirm that Niobium has been distributed in the alloy during the melting process. The EDS result was obtained by scanning the signal in a specific region of the sample, and the obtained peak indicates semi-quantitatively the presence of Nb at several points. Different results for the EDS would permit the identification of Nb presence at different points in the sample, so that the distribution of Nb can be inferred.

This result is consistent with previous diffractometry where no precipitated β phases of Nb were identified. Different authors, such as Lelievre [19] and Neogy [20], reported that the α-*Zr* matrix contains approximately 0.67% of substitutional atomic *Nb* in the solid solution and is free of precipitated β-*Nb*. The results of X-ray diffraction presented in this paper are completely consistent with such an assertive.

4. Conclusion

Both Zirconium and Niobium have been used to form alloys known as *Zr1Nb* that were thoroughly analyzed with the assistance of different techniques. After various tests, it was possible to determine the following parameters for the melting process: Voltage, Current, Pressure, Gas Flow and Fusing Time. Using a non-consumable electrode fusion furnace, it was possible to obtain such alloys with sufficient degree of homogeneity high enough to be used in nuclear applications as well as for the continuation of our characterization working processes.

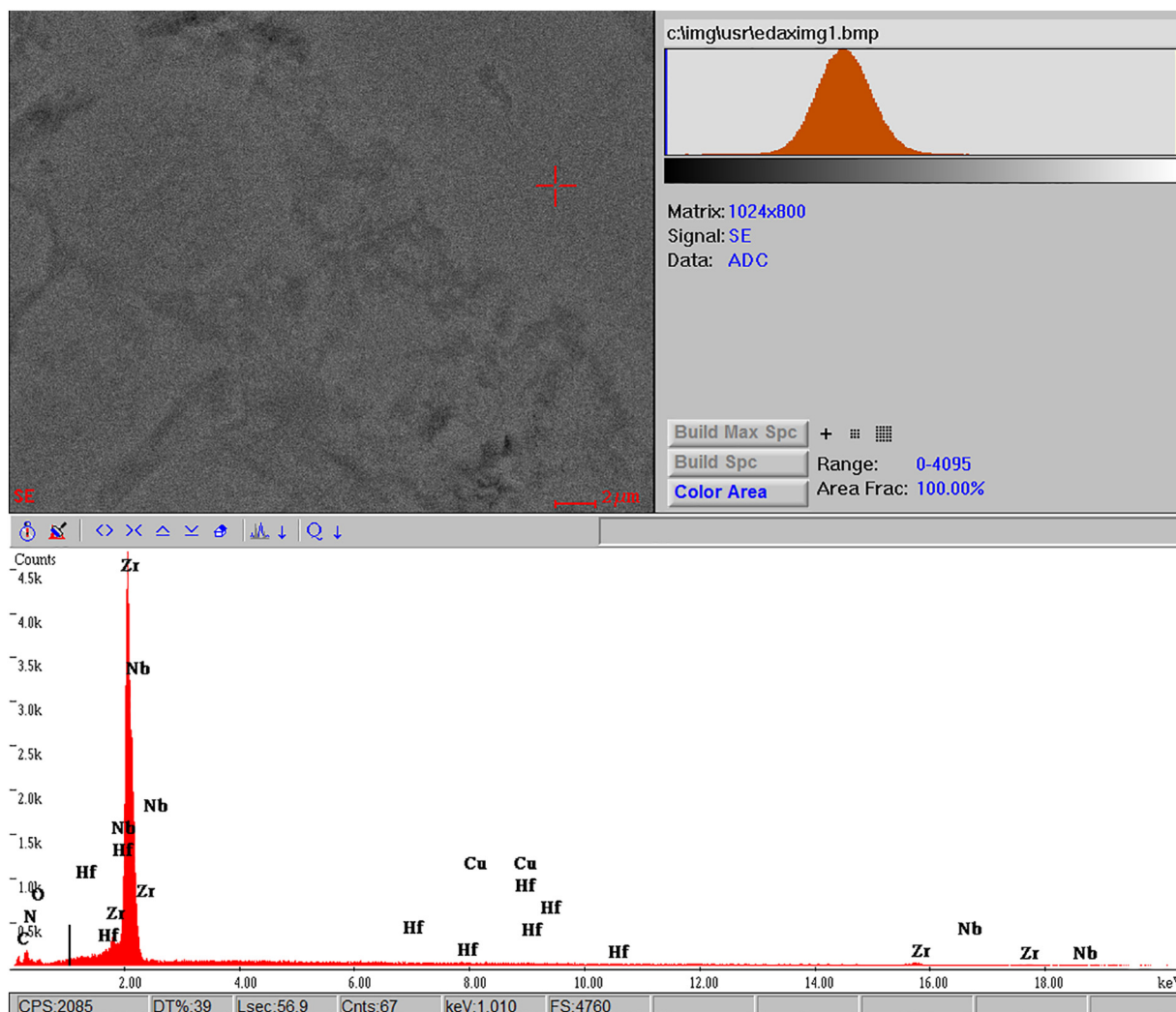The results of X-ray diffraction for phase identification led to

Table 2
Quantitative results for a *Zr1Nb* sample obtained after hot rolling.

Element line	Net counts	Z	A	F	Weight %	Atomic %
C K	3690	0.000	0.000	0.000	–	–
Zr K	28879	0.000	0.000	0.000	–	–
Zr L	240703	1.000	1.000	1.000	99.32	99.33
Zr M	0	0.000	0.000	0.000	–	–
Nb K	553	0.000	0.000	0.000	–	–
Nb L	1731	0.994	0.961	1.000	0.68	0.67
Nb M	203	0.000	0.000	0.000	–	–
Total					100.00	100.00

Fig. 9. A typical result of EDS obtained for the *Zr*1*Nb* sample after hot rolling.

conclude that the *Zr*1*Nb* alloys before and after hot rolling have the same HCP crystalline structure, exhibiting only the homogeneous α-*Zr* phase, and pointing that the β-*Nb* phase is not present. This is an indication that the *Nb* is in solid solution in the crystalline structure of the *Zr*1*Nb* alloy.

The results of optical microscopy showed variations in the porosity and in the orientation of dendrites before and after the heat treatment, performed at 1273 K for 2 h. Analysis of SEM realized after hot rolling showed that our *Zr*1*Nb* alloy samples present only the primary α-*Zr* phase. The samples also present good homogeneity in spite of the deformations along the horizontal direction induced by the rolling mill cylinders. The EDS analysis showed a semi-quantitative value of 0.67% *Nb* mass in the *Zr*1*Nb* alloy after hot rolling, consistent with the solubility limit of the solid *Nb* in the *Zr* matrix.

Therefore, controlling the melting and hot rolling parameters, it was possible to obtain a *Zr*1*Nb* alloy with a high degree of homogeneity and purity. The next move of our research consists in doing dynamical mechanical analysis - DMA of such alloys. Goals are to determine their inelastic proprieties, such as elasticity or Young's modulus, temperature and peak frequency, defect combinations and internal friction. These studies will be conclusive about the possibility to use this alloy on the fabrication process of fuel pipes of low power reactors.

Acknowledgment

References

[1] ASTM B551/B551M – 07, Standard Specification for Zirconium and Zirconium Alloy Strip, Sheet and Plate, Annual Book of ASTM Standards.

[2] ASTM A516-70, Standard Specification for Pressure Vessel Plates, Carbon Steel, for Moderate and Lower-Temperature Service, Annual Book of ASTM Standards, Vol. 01.04, ASTM International, West Conshohocken, PA, 2010, pp. 510–520.

[3] B. Derby, M.F. Ashby, On dynamic recrystallization, Scr. Metall. 21 (1987) 879–884.

[4] O.N. Senkov, J.J. Jonas, F.H. Froes, Steady flow controlled by the velocity of grain boundary migration, Mater. Sci. Eng. A A225 (1998) 49–53.

[5] R. Peter, K. Bruce, Zirconium in the nuclear industry, ASTM - Fourteenth International Symposium, 2006.

[6] U. S. Nuclear Regulatory Commission Office of Nuclear Regulatory Research Washington, (2004).

[7] B. Cox, Some thoughts on the mechanisms of in-reactor corrosion of zirconium alloys, J. Nucl. Mater. 336 (2005) 331–368.

[8] R. Kapoor, J.K. Chakravartty, Characterization of hot deformation behavior of Zr2.5Nb in b phase, J. Nucl. Mater. 306 (2002) 126–133.

[9] Y.H. Jeong, H.G. Kim, T.H. Kim, Effect of β-Phase, precipitate and Nb-concentration in matrix on corrosion and oxide characteristics of ZrxNb Alloys, J. Nucl. Mater. 317 (1) (2003) 1–12.

[10] J.D. Robson, Modelling precipitation in zirconium niobium alloys, J. Nucl. Mater. 377 (3) (2008) 415–422.

[11] R. Jerlerud Perez, A.R. Massih, Thermodynamic evaluation of the Nb–O–Zr System, J. Nucl. Mater. 360 (3) (2007) 242–254.

[12] A.C. Souza, J.L. Rossi, P. Tsakiropoulos, L.G. Martinez, C.R. Grandini, F.C. Ceoni, C.S. Mucsi, H.P.S. Correa, Preparation and melting of Zr1Nb alloy, Mater. Sci. Forum 869 (2016) 578–584.

[13] ASTM A516-70, Standard Specification for Pressure Vessel Plates, Carbon Steel, for Moderate and Lower-Temperature Service, Annual Book of ASTM Standards, Vol. 01.04, ASTM International, West Conshohocken, PA, 2010, pp. 281–284.

[14] C.R. Grandini, W. Govedise, A.C. Borges, Projeto e Construção de um Sistema para Tratamentos Térmicos em Ultra-Alto-Vácuo, I Brazilian Conference on Themes of Thermal Treatments, Indaiatuba, Sao Paulo, Brazilian Ceramics Association, 2003, pp. 391–401.

[15] S. Neogy, D. Srivastava, G.K. Dey, J.K. Chakravartty, S. Banerjee, Annealing studies on Zr-1Nb and Zr-1Nb-1Sn-0.1Fe alloys, Trans. Indian Inst. Metals 57 (5) (2004) 509–519.

[16] P. Liang, N. Dupin, S.G. Pries, H.J. Seifert, I. Ansara, H.L. Lukas, F. Aldinger, Thermodynamic assessment of the Zr-O binary system, Z. Met. 92 (2001) 747–756.

[17] J.P. Abriata, J. Garces, R. Versaci, The O-Zr (Oxygen-Zirconium) system, Bull. Alloy Phase Diagr. 7 (2) (1986) 116–224.

[18] A. Fernandez-Guillermet, W. Huang, Calphad estimates of the lattice stabilities for high melting bcc metals: V, Nb und Ta, Z. Met. 79 (1988) 88–95.

[19] G. Lelievre, Étude du rôle des précipités intermétalliques dans l'absorption d'hydrogène lors de la corrosion aqueuse d'alliages de Zirconium (Ph. D. Dissertation), Joseph Fourier University, Grenoble, France, 1998.

[20] S. Neogy, D. Srivastava, R. Tewari, R.N. Singh, G.K. Dey, S. Banerjee, Microstructural study of hydride formation in Zr1Nb alloy, J. Nucl. Mater. 322 (2003) 195–203.